A structural perspective on the temperature-dependent activity of enzymes

Authors: Matthew J. McLeod[1]*, Sarah A. E. Barwell[2], Todd Holyoak[2], Robert Edward Thorne[1]

Affiliations:

[1]Cornell University, Ithaca New York, USA. Department of Physics.

[2]University of Waterloo, Waterloo Ontario, Canada. Department of Biology.

*Corresponding author. Email: mjm758@cornell.edu.

ABSTRACT: Enzymes are biomolecular catalysts whose activity varies with temperature. Unlike for small-molecule catalysts, the structural ensembles of enzymes can vary substantially with temperature, and it is in general unclear how this modulates the temperature dependence of activity. Here multi-temperature X-ray crystallography was used to record structural changes from −20°C to 40°C for a mesophilic enzyme in complex with inhibitors mimicking substrate-, intermediate-, and product-bound states, representative of major complexes underlying the kinetic constant k_{cat}. Both inhibitors, substrates and catalytically relevant loop motifs increasingly populate catalytically competent conformations as temperature increases. These changes occur even in temperature ranges where kinetic measurements show roughly linear Arrhenius/Eyring behavior where parameters characterizing the system are assumed to be temperature independent. Simple analysis shows that linear Arrhenius/Eyring behavior can still be observed when the underlying activation energy / enthalpy values vary with temperature, e.g., due to structural changes, and that the underlying thermodynamic parameters can be far from values derived from Arrhenius/Eyring model fits. Our results indicate a critical role for temperature-dependent atomic-resolution structural data in interpreting temperature-dependent kinetic data from enzymatic systems.

One-Sentence Summary: Structural data spanning a 60°C temperature range for enzyme complexes mimicking the substrate-, intermediate-, and product-bound states illuminate how small temperature-dependent structural changes may modulate activity and render parameters deduced from Arrhenius/Eyring plots unreliable.

INTRODUCTION

Chemical reaction rates increase with temperature. For small-molecule catalysts and substrates, increased rates are associated with increased collision velocities and frequencies arising from increased kinetic energy. For enzyme-catalyzed reactions, additional temperature variation in rates may occur due to changes in the conformational ensembles of the enzyme and substrate. Temperature-dependent enzyme reaction rates are typically measured under saturating substrate conditions, where active sites are fully occupied. Turnover (k_{cat}) then reports only on steps after formation of the enzyme-substrate (ES) complex and is independent of collision frequency, and effects of increased kinetic energy will only be observed for processes that occur after formation of ES through to product release and regeneration of the free enzyme (E + P).

Despite these and other significant mechanistic differences, analysis of k_{cat} as a function of temperature for enzymatic systems is typically based on Arrhenius or Eyring-Polyani (E-P) formalisms, which were derived from small molecule studies and assume the underlying thermodynamic parameters ($\Delta H, \Delta S$) are temperature-independent. However, enzymatic Arrhenius/Eyring plots can be more complex than their small molecule counterparts. For example, they may be linear at lower temperatures and then curve downward at elevated temperatures, with rates k_{cat} rapidly decreasing above a temperature T_{opt}. This downward curvature is most often

attributed to unfolding, and but may be observed even at temperatures well below the unfolding temperature.(for ex. see 1–6)

Three models have been proposed to describe this latter behavior: Macromolecular Rate Theory[1], the Equilibrium Model[7] and a model described by Roy, Schopf and Warshel[6]. Macromolecular Rate Theory (MMRT) suggests that the temperature dependence of enzymatic rates is controlled by the heat capacity change between two states that determine activity.[1,8–11] Rigidification of the enzyme ensemble as it traverses the conformationally restricted transition state results in a negative heat capacity difference $\left(\Delta C_p^{\ddagger}\right)$ and downward curvature of the Arrhenius plot after T_{opt}.[1] The Equilibrium Model suggests that downward curvature is due to a shift of the equilibrium defining an enzyme's conformational ensemble toward increasing population of inactive states as temperature is increased, prior to denaturation.[7] The third model suggests that the more polar GS is more conformationally restricted than the less polar TS.[6] As temperature increases, there is a loosening of the GS that increases its entropy, leading to a decrease in $\Delta S^{\ddagger}$, an increase in $\Delta G^{\ddagger}$ and downward curvature. The first two of these models have been the most discussed, with evidence from kinetic measurements, molecular dynamics simulations, theoretical analysis, and model fitting providing support for each. Testing these models requires observation of functionally relevant changes in conformational ensembles along the reaction coordinate as temperature is changed. More generally, such observations are required to understand observed rate-temperature relationships.

A powerful approach to probing temperature-dependent enzyme structure-activity connection is to determine atomic/near atomic resolution X-ray crystallographic structures over a wide temperature range where enzymes exhibit activity. Ideally, the temperature range should span the lower biological limit of roughly −20°C to the denaturation/unfolding temperature,[15] and the

crystal form should allow sufficient conformational flexibility to preserve activity. Robust methods for collecting high-quality structural data from "native", cryoprotectant-free crystals that maintain liquid internal solvent at temperatures down to ~200 K (-73 °C) have been established.[16,17] Methods and hardware for collecting data with minimal crystal dehydration or degradation at up to ~90°C have also been demonstrated.[18] This ~160°C data collection temperature range, feasible at high-resolution with X-ray crystallography, is currently difficult to match using any other structural probe. Despite this, only a handful of multi-temperature crystallography studies spanning a mechanistically useful temperature range have been reported.[19–26] A recent publication identified only 11 published crystallographic structures at temperatures above 37°C.[27]

Here we performed crystallography at -20, 0, 20, and 40°C to probe a mesophilic, GTP-dependent phosphoenolpyruvate carboxykinase from rat cytosol (rcPEPCK) that retains activity in its crystalline form. To observe changes in structure related to k_{cat}, we used complexes representing three states on the reaction coordinate that comprise k_{cat} (**Scheme 1**).[28,29]

rcPEPCK has been extensively studied both kinetically and structurally, revealing a clear picture of molecular events leading to activity, allowing temperature-dependent changes to be assessed for their impact on activity.[28–34] PEPCK is a metabolic enzyme that interconverts oxaloacetic acid (OAA) and phosphoenolpyruvate (PEP) using a metal-cofactor involved in binding and catalysis (M1, typically Mn^{2+} - **Fig. S1**), a second nucleotide-associated metal (M2, typically Mg^{2+}), and a phosphoryl donor (either GTP, ATP, or PP_i depending on PEPCK class).[35] With respect to the reversible reaction, the data are consistent with a stepwise mechanism where, in the direction of PEP synthesis (OAA→PEP), the reaction is initiated by the decarboxylation of OAA creating an enol-pyruvate intermediate. This intermediate is subsequently phosphorylated

by the phosphoryl donor producing PEP (**Scheme 1**).[reviewed in 35] Substrate binding and activity have been shown to be coupled to several dynamic transitions in the enzyme, including a global closure via rotation of the N- and C-terminal domains that reduces the active site cavity's total volume, as well as loop and residue rearrangements.[32] More specifically it has been shown that the R-(substrate-binding) and P-(nucleotide-binding) loops undergo disorder-to-order transitions upon binding, aiding in orienting the substrate and nucleotide appropriately.[32] The Ω-loop, an active site lid, undergoes a similar essential disorder-order transition as it folds and closes over the active site and is held in place by the adjacent R-loop after the enzyme has undergone substrate-induced global closure and active site remodeling (**Fig. 1**).[31,33,36] Lid closure has been shown to be essential to PEPCK function as the lid holds the active site and substrates in a catalytically competent state and protects the enol-pyruvate intermediate from solvent-mediated protonation and the non-productive formation of pyruvate.[36]

Our temperature-dependent structural characterization of rcPEPCK, as well as other previous works indicating structural changes with varying temperature[19,20,22,37,38], prompted us to re-evaluate assumptions made in applying Arrhenius / Eyring-Polanyi (E-P) models to temperature-dependent enzyme kinetic data. Although Arrhenius/E-P plots provide a qualitative descriptor of an enzyme's free-energy landscape, combined multi-temperature structural and kinetic/biochemical measurements are required for quantitative and mechanistic insight.

RESULTS

Multi-temperature kinetics. An Eyring-Polyani (E-P) plot of k_{cat} for rcPEPCK in the reverse, PEP→OAA, direction (**Fig. 2,** raw data in **Data S1**) showed a decreasing slope with increasing temperatures above ~25°C (**SI Data S2**), with a maximum rate at ~50°C (T_{opt}) and a loss of activity at higher temperatures. In the presence of viscogen (glycerol) at constant viscosity (2.4 cp/mPa),

k_{cat} decreased at temperatures above ~50°C but was unaffected at lower temperatures. k_{cat} / K_M for the PEP→OAA reaction was determined at four temperatures between 15°C and 55°C (**SI Table S1)** but the data are not sufficient to assess the functional variation with temperature. k_{cat} for the OAA→PEP direction could not be reliably determined above 35°C as the non-enzymatic rate of metal-catalyzed decarboxylation of OAA became significant. An Arrhenius plot of the available data (7-37°C) appeared roughly linear (data not presented).

Multi-temperature crystallography. While all three complexes examined here were inhibited complexes using mimics for the OAA/PEP substrates, structural evidence using authentic substrates with WT and mutant forms of the enzyme suggest that the conformational states sampled in these complexes faithfully reproduce those of the catalytically competent enzyme-substrate complexes (**Fig. 1 and SI Fig. S2**).[28,29,34,39] In the oxalate(OX)-GTP and phosphoglycolic acid (PGA)-GDP complexes CO_2 is not present. Therefore, the PGA-GDP complex represents a partially occupied encounter/product complex (prior to CO_2 binding / after CO_2 is released) and the OX-GTP complex represents the intermediate state which may or may not have CO_2 present in the authentic enolate-GTP complex but is still conformationally closed. Therefore, both these complexes represent meaningful states along the catalytic trajectory.[28,39]

rcPEPCK β-sulfopyruvate (βSP)-GTP complex (Scheme 1, Complex 1). Both βSP and GTP were fully occupied in the active site at all temperatures. For GTP, the electron density indicated two resolvable conformers between –20°C and 20°C (**Fig. 3**). One conformer was modeled in a fixed position that has been clearly resolved in the open PEPCK-GTP complex at cryogenic temperatures, and is deemed incompetent for phosphoryl transfer (**IC** in **Fig. 3**).[29] The electron density suggests the other conformer changes pose with temperature, and at 40 °C adopts a conformation that has been observed in cryogenic structures of the closed, oxalate-GTP complex,

deemed competent for phosphoryl transfer (**C** in **Fig. 3**).[28,30] At 40°C, there is only evidence for the closed oxalate-GTP complex conformer. The conformation change of GTP occurs by a rotation of both the α-phosphate and ribose out of the plane of the triphosphate moiety. Occupancy refinements, when the B-factors are fixed to the proteins average B-factor, shows the fixed PEPCK-GTP complex conformer is depopulated while the rotating oxalate-GTP like conformer is populated with temperature (**Fig. 3**). The occupancies for IC:C conformers are 72%:28% at -20°C, 52%:48% at 0°C, 39%:61% at 20°C, and 0%:100% at 40°C. The change in nucleotide conformation was coupled to movement of the P-loop as it shifted towards the M1 metal with increasing temperature - a process previously associated with enzyme/lid closure in cryogenic structures (**SI Fig. S3**).[28,29,40] These adjustments lead to various increases and decreases in interatomic distances between GTP and contacting residues (**SI Fig. S4**). Electron density in the ordered Ω-loop conformation was observed to increase between –20°C and 0°C, remained nearly constant between 0°C and 20°C, and diminished at 40°C (where overall resolution was worse), hinting at possible disordering of the lid at 40°C and above (**Fig 4, Table S2,** and **Fig. S5** for βSP-GTP Ω-loop electron density at lower contour). Over the –20°C to 20°C temperature range where data set resolution was nearly constant, the normalized B-factors ($B\text{-factor}_{res}$-$B\text{-factor}_{protein}$) of residues 94-134 and 228-251, increased with increasing temperature while those of residues 59-93, 255-303, 413-420, 535-557, and 579-590 decreased (**SI Data S3**). The normalized B-factors for the Ω-loop are consistent with increased order with increasing temperature between –20°C to 20°C evident in the electron density maps.

rcPEPCK oxalate (OX)-GTP complex (enol-pyruvate-GTP) (Scheme 1, Complex 2). In contrast to the temperature-dependent changes noted for the βSP-GTP complex **(Complex 1)**, a single dominant/resolvable conformer of oxalate and GTP was modeled at all temperatures. The solvent-exposed O2' of the ribose sugar (**SI Fig. S6**) and adjacent atoms showed a significant

increase in B-factor with increasing temperature, consistent with this region of the nucleotide becoming disordered rather than populating a new conformation. The lack of movement in the triphosphate portion is correlated with a single dominant/resolvable conformation of the P-loop at all temperatures (**SI Fig. S3**). Strong electron density for the Ω-loop was present at all temperatures (**Fig. 4**) although a slightly larger B-factor may suggest increased disorder at 40°C (**SI Table S2**). Consistent with prior cryogenic structures, at all temperatures the OX-GTP complexes had a PEG molecule bound in a cavity between the N- and C-terminal domains of PEPCK; a loop formed by residues 149-154 changed position to accommodate the PEG. In both the βSP-GTP and PGA-GDP complexes, the cavity region was partially disordered but in the dominant/resolved conformation the loop closed off the cavity to prevent PEG binding (**Fig. S7**). B-factor analysis indicates some minor temperature dependencies in peripheral regions of the enzyme in this complex. (**SI Data S3**). Residues 95-125 show increased disorder while residues 265-300 show increased order with increased temperature.

rcPEPCK phosphoglycolic acid (PGA)-GDP complex (PEP-GDP) (Scheme 1, Complex 3). Like the OX-GTP complex, in the PGA-GDP complex at all temperatures, GDP was fully occupied in the active site and single dominant/resolved conformations of the P-loop and nucleotide were observed (**SI Fig. S3**). The O3' and other ribose atoms exhibited local temperature-dependent disorder (**SI Fig. S6**), as in the OX-GTP complex. PGA, on the other hand, exhibited significant conformational change with temperature (**Fig. 5** and **Fig. S2 & 8**). PGA (and PEP) are known to adopt three discrete conformations.[28,34,39] Two of these exhibit second sphere coordination to the M1 cation and positions the phosphate at too great a distance from the β-phosphate of GDP for phosphoryl transfer to occur, and are thus deemed catalytically incompetent (IC1, IC2) (**Fig. 5** and **Fig. S2 & 8**).[39] In the third conformation, PGA (PEP) directly coordinates to the M1 metal, and the phosphate is positioned in the same location as the γ-phosphate of GTP

that is unoccupied when GDP is bound, and is therefore the catalytically competent conformation (C1, **Fig. 5** and **Fig. S2 & 8**).[28,34] At –20°C, IC1 and IC2 were fully occupied with a distribution of 40%:60%:0% (IC1:IC2:C1), and shifted to a 50%:50%:0% distribution at 0°C. At 20°C, C1 became populated with a 0%:55%:45% distribution, and at 40°C the shift toward the competent state was nearly complete with a 0%:25%:75% distribution. Concomitant with this binding mode change, Y235 shifted from a buried conformation when the incompetent conformations were dominant and rotated toward the active site as the competent conformation was populated (**Fig. 5D)**. The Ω-loop made a similar shift: it largely occupied the open, disordered state at –20°C, and became increasingly ordered and closed as temperature increased (**Fig. 4**). The only indication of temperature dependency from normalized B-factors was the increase in order of the Ω-loop as temperature increased (**SI Data S3**).

DISCUSSION

The significance of crystallographic findings depends on constraints imposed by the crystal lattice and how these modify the ensemble of accessible conformational states relative to those of the enzyme in solution. Prior characterization of rcPEPCK crystals has found that the lattice allows multiple conformational states to be observed. For example, all catalytically relevant domain and loop motions including the transition between open and closed states upon soaking with substrates or inhibitor mimics are allowed. The rich history of structure-function investigations of rcPEPCK provides a basis for interpreting temperature-induced changes.[28–35,39,41–44] Furthermore, a simplified approach to time-resolved crystallography has recently revealed the hypothesized active conformation of PEP (*vida infra*, competent 1 (C1) conformation) generated from OAA and GTP, confirming that rcPEPCK is active *in crystallo* and that all dynamic modes necessary for activity are accessible (**SI Fig. S2**).[34]

Temperature increases global B-factors but has variable and complex-dependent local effects. Nearly all previous "more than one" multi-temperature crystallographic studies have focused on comparison of room temperature ~298 K (25°C) and cryogenic temperature ~100 K (–173 °C) structures. These studies have revealed significant changes in the structural ensemble associated with cryocooling and indicate the importance of measuring structures at physiological temperatures in assessing structure-function relationships.[21,23–25,45–48] Data collected at temperatures above 100 K and below ~220 K (–53°C) (near and below the protein-solvent dynamical (or glass) transition, where most functionally salient protein and solvent dynamics are absent) usually add limited information of relevance to understanding mechanism beyond that available at 100 K.[20] Where crystallographic data at several temperatures above the dynamic transition has been collected, only the apo / holo form and one additional complex have been examined, rather than a larger set of complexes representing states along the reaction coordinate.[19,20,22,26,49] Multi-temperature cryoEM studies, where grid-containing samples are prepared at different temperatures immediately prior to cryocooling, have examined two systems and revealed domain-scale changes and changes in the ligand pose.[37,38] For one system only the apo complex and the ternary "transition state" like complex[37] were examined, at 6 temperatures between 4°C and 70°C and resolutions between 2.1 and 3.0 Å.[37] For the other system, wild-type and mutant versions of a single complex were examined at temperatures of 4, 37 and 42 °C and resolutions of 4.1 - 5.2 Å. Unlike in multi-temperature crystallography where the target temperature is maintained during data collection, multi-temperature cryoEM requires freeze-trapping which perturbs the conformational ensemble. Even though cooling rates of thin-film cryoEM samples are one to two orders of magnitude larger than can be achieved with microcrystals, substantial relaxation of side chains and smaller moieties is still expected, and

sample precooling in cold gas present immediately above the liquid ethane introduces uncertainty in the trapped temperature.

Previous multi-temperature structural studies revealed two general phenomena which the present data support. First, global average B-factors increase as temperature increases, primarily reflecting increased thermal fluctuations rather than increased static disorder.[20–22,50] Second, the effects of temperature on the dynamic behavior of local structural elements such as residues and loops depend on the local context of neighboring residues, charge distributions/pKas, solvation, steric interactions, etc. Both increases and decreases in order with increasing temperature are observed.[19–21,23]

Here, the global B-factor for each of three sampled rcPEPCK complexes comprising k_{cat} increased with increasing temperature (**SI Data S4**). Each complex has a unique temperature dependence, with local disorder either increased or decreased depending on the region examined (**SI Data S3**). The intermediate OX-GTP complex was the most temperature agnostic, as the global B-factor showed only a small change and the Ω-loop and substrates did not show clear changes in position or occupancy with temperature. In contrast, both the forward (βSP-GTP) and reverse (PGA-GDP) GS complexes showed an increase in Ω-loop (active-site lid) order with increasing temperature, with additional ordering in the PGA-GDP complex but increased disorder in the βSP-GTP complex observed at 40°C (**Fig. 4, Table S2** and **Fig. S3**). There was also an increase in the normalized B-factor (**Table S2**) of the Ω-loop of the OX-GTP complex at 40°C, but this does not translate to significantly more disorder (**Fig. 4**). Coincident with increasing lid order, the P-loop and nucleotide conformations in the βSP-GTP complex change (**Fig. 3 and Fig. S3)**. At 40°C, GTP adopts an eclipsed, competent conformation; the γ-phosphate becomes a better leaving group, thus promoting phosphoryl transfer and turnover.[28,40] This eclipsed geometry

is similar to that observed in the intermediate state (OX-GTP) (**Fig. 3).** Although this conformational change which aids phosphoryl transfer (second chemical step) occurs in the βSP-GTP complex, before decarboxylation (the first), it will still result in an increase k_{cat}. At high temperatures, phosphoryl transfer can immediately follow decarboxylation because GTP is already in the eclipsed geometry. In contrast, at low temperatures, after decarboxylation GTP must undergo an energetically costly conformational change to the eclipsed state before phosphoryl transfer can occur. This additional conformational change results in an increased time for turnover. In the PGA-GDP complex, PGA shifted from predominantly populating the two incompetent conformations (IC1 and IC2) below 20°C toward increasing occupancy of the competent state at 20 and 40°C — a conformational shift that is required for phosphoryl transfer (C1) (**Fig. 5** and **SI Fig. S8**).

Multi-temperature crystallography reveals structural changes influencing kinetic parameters. The observed structural changes are directly supported by previous structure-function studies indicating similar changes when rcPEPCK traverses its reaction coordinate.[28–31] Together with results from previous cryoEM studies[37,38], the present results sampling enzyme-ligand complexes corresponding to known states comprising k_{cat} suggest that the equilibrium between conformational states shifts so that the population of active states increases with increasing temperature up until some maximum, T_{opt}.

This increase in active state population likely contributes to the observed increase in k_{cat} with temperature, as this parameter reflects the energetic barriers of all events on the reaction coordinate following the formation of the enzyme-substrate complex.[51] If one of these events has a *significantly* slower rate than the others, k_{cat} will be *mostly* controlled by that event and following events; this is often simplified by assuming that k_{cat} represents this one event. However, in

measurements over a large temperature range (e.g., from ~280 K to 340 K), temperature-dependent structural changes may differentially affect the individual microscopic steps and their relative contributions to k_{cat}, as seen in the different temperature variations of the Ω-loop in each sampled complex. Here, significant differences in the structural data in response to changing temperature of inhibitor complexes representing three meaningful states on the reaction coordinate are observed. These data indicate changes that may plausibly impact rate-determining step(s) at low and high temperatures.Alternative possibilities that could impact rate-determining steps include changes to the dominant reaction mechanism itself, perhaps involving an increase in occupancy of competent conformers with occupancies too low to be discerned in our maps; and changes in the TS structure with temperature.

A previous mutational and kinetic study found that rcPEPCK is at least partially rate-limited by phosphoryl transfer (at ambient temperature).[33] The present structural data support this conclusion, as the structural changes observed (eclipsed phosphate geometry of GTP, PGA conformation changing to coordinate with M1, lid closure allowing for chemistry) with increasing temperature all lead to a shift in conformational state that is more favorable for phosphoryl transfer.

The intermediate state, represented here by the OX-GTP complex, is resistant to temperature-induced changes. This is not surprising, as the conformational ensemble of this complex must be tightly constrained for the reaction to proceed. Prior work demonstrated that under conditions where the Ω-loop opens prior to phosphorylation of the enolate intermediate, solvent can protonate the intermediate to form a side product, pyruvate.[31] PEPCK likely evolved to ensure robust loop closure throughout the chemical steps essential to maximize the enzyme's efficacy, consistent with the conformational stability observed for the OX-GTP complex. The induction of the closed conformation in the OX-GTP complex is likely aided by rotation of Y235, as all other active site

residues have largely the same positions in the βSP-GTP and OX-GTP complexes (**Fig. S8**)[28], by a redistribution of interaction distances at the active site (and beyond), and by the physicochemical properties of the ligand itself.

Increased local disorder in the product-complex suggests a new rate-limiting step at high temperatures. Arrhenius / E-P plots of $k_{cat}(T)$ for rcPEPCK exhibit non-linear behavior at high temperature, with negative curvature leading to a maximum value for $k_{cat}(T)$ at a T_{opt} of ~50°C and slope inversion at temperatures above T_{opt}. As mentioned previously, this non-Arrhenius behavior near T_{opt} is common in enzyme systems, and recent efforts have attempted to create a generalizable model describing it.[1–3,5,6,13,14,52,53] Based upon these efforts, negative curvature at temperatures near T_{opt} may be attributed to 1) a change in mechanism, 2) an increase in the barrier that limits rates at high temperatures, or 3) a new barrier along the reaction coordinate becoming dominant. For rcPEPCK, significant downward curvature, starting near ~40°C, coincides with k_{cat} exhibiting sensitivity to solvent viscosity (~50°C). A possible interpretation is that a new, non-chemical rate-limiting step has emerged (**Fig. 2**). Structures at 40 °C provide weak evidence of a shift to product release as the rate limiting step, which would be consistent with a high-temperature viscosity dependence of k_{cat}. Under these assumptions, we speculate that lid ordering prior to chemistry may then become increasingly unfavorable, and this dynamic (and presumably solvent friction-sensitive) step could become rate limiting.

Attempts to obtain high-resolution crystallographic data at temperatures above 40°C were not successful due to crystal instability. However, structures at 40°C provide weak evidence that a shift to product release as the rate limiting step may play a role in the high-temperature viscosity dependence of k_{cat}. For the PEP→OAA reaction direction, at 40°C the Ω-loop in the βSP-GTP

(product) complex shows hints of increased disorder: a loss of ordered density (**Fig. 4 and Fig. S5**) in the loop and an increase in B-factor that is larger than expected based solely on the lower resolution of the 40°C data set (**Table S2**). Disordering of the Ω-loop should aid in product release thus increasing k_{cat}. In the PGA-GDP (substrate) complex, the lid remains closed at 40°C. Given that the Ω-loop has no direct interaction with either the product or substrate complex, it seems plausible that, like the βSP-GTP complex, disorder in the lid may develop above 40°C. Under these assumptions, we speculate that lid ordering prior to chemistry may then become increasingly unfavorable, and this dynamic (and presumably solvent friction-sensitive) step could become rate limiting. Alternatively, new high-temperature conformers may arise which can specifically bind glycerol. This binding may then increase the fraction of inactive conformers. These hypotheses can be tested with molecular dynamics simulations.

Linear Arrhenius plots hide a changing free-energy landscape that is revealed through multi-temperature crystallography. The temperature dependent activity of related enzymes (e.g., two mutants) is often compared using Arrhenius or Eyring plots. Activation / thermodynamic parameters are extracted from the slope and *y*-intercept of linear fits. These plots typically report a modest number of data points, each with significant experimental uncertainty, acquired over a limited temperature range. Uncertainty in the slope of such fits arises both from measurement uncertainties and from using a linear fit when the underlying variation may be nonlinear. Uncertainties in the *y*-intercept are particularly large, as a fit to data spanning, e.g., 0.003 K^{-1} <1/T<0.0037 K^{-1} must be extrapolated over more than four times that interval to 1/T=0.[54]

An implicit assumption in applying the Arrhenius and Eyring models is that, when k_{cat} (or k_{cat}/T varies linearly with temperature over some range, as is the case at low temperature for rcPEPCK, the thermodynamic parameters describing the system are temperature-independent.

Thus, a single "apparent" activation entropy $\Delta H^{rxn,app}$ and enthalpy $\Delta H^{rxn,app}$ (delineated from the true values ΔS^{rxn} and ΔH^{rxn})) are assumed. This may be a reasonable assumption in small-molecule reaction kinetics. However, hydrophobic interactions, pK_a values, and other properties/interactions of relevance to protein structure and dynamics are temperature dependent.

As is clear from this and previous multi-temperature structural studies, enzyme structure is temperature dependent. Here we have observed functionally relevant changes in inhibitor-bound active site structures mimicking the complexes sampled by with k_{cat} even in temperature ranges where the corresponding kinetics plots appear to be strictly linear (**SI Data S2**). Based on these observations for enzyme systems, there is no reason to expect the underlying thermodynamic parameters to remain constant over the temperature ranges typically probed in kinetics experiments.

Interpretation of kinetics measurements. As will be discussed in more detail elsewhere, a linear E-P fit to the rcPEPCK data (implicitly assuming a temperature-independent free-energy landscape) (**Fig. 2**) between 8°C (281 K) and 25°C (298 K) gives $\Delta H^{rxn,app} = 26.3 \pm 0.85$ kcal/mol and $\Delta S^{rxn,app}$ = 0.037 ± 0.003 kcal/mol•°C (R^2=0.997). Identical fits to the rcPEPCK data can be obtained by assuming that ΔH^{rxn} at 8°C is 21.30 kcal/mol (19% smaller) and decreases with increasing temperature at a rate of 0.0178 kcal/mol•°C (i.e., by ~0.25 kcal or ~1/4 of a hydrogen bond over 14 °C) and a constant ΔS^{rxn} = 0.019 kcal/mol•°C (48% smaller); or by assuming that ΔH^{rxn} at 8°C is 16.3 kcal/mol (39% smaller) and decreases with increasing temperature at a rate of 0.035 kcal/mol•°C (i.e., by ~0.5 kcal or ~1/2 of a hydrogen bond over 14 °C) and a constant ΔS^{rxn} = 0.016 kcal/mol•°C (96% smaller). In fact, there is a wide range of physically plausible combinations of linearly varying enthalpies $\Delta H^{rxn}(T)$ and fixed entropies ΔS^{rxn} (or of simultaneously varying enthalpies and entropies) that can recapitulate the E-P fit to the activity

data. In other words, the observed slope and intercept of Arrhenius or E-P plots of $k_{cat}(T)$ constrain but do not determine the underlying enthalpies $\Delta H^{rxn}(T)$ and entropies $\Delta S^{rxn}(T)$ and their temperature dependencies that determine the observed k_{cat}.

This analysis indicates that small temperature variations of underlying thermodynamic / reaction parameters may, in the absence of near-atomic resolution multi-temperature structural information and/or support from other measurements, make quantitative and even qualitative interpretation of parameters derived from Arrhenius / E-P fits to enzyme kinetic data unreliable, with significant consequences for mechanistic interpretations. Qualitative ordering of, e.g., mutant enzymes based on their Arrhenius / Eyring slopes and intercepts may be unreliable.[48,55–59] Kinetics data only yields $\Delta G^{rxn}(T)$, a composite of temperature-dependence, and unknown enthalpy and entropy.

CONCLUSION

Stochastic thermal fluctuations of an enzyme-substrate complex drive the crossing of energetic barriers. Unlike in small molecule catalysis, in enzymes the relevant enthalpy and entropy changes must vary with temperature due to an enzyme's many degrees of freedom and lability, the many steps along the reaction coordinate[60] contributing to the overall $\Delta G^{rxn}(T)$, and the temperature variations of physicochemical interactions that govern enzyme structure and activity. Together, these modulate the temperature-dependent activity that would be otherwise be observed if the enzyme were fully "locked down", with the loss of activity accompanying high temperature unfolding being the most obvious example. Consequently, analysis of kinetic data based on specific mechanistic assumptions (e.g., a temperature-independent free-energy landscape) may be confounded by gradual variations of underlying parameters (ΔH^{rxn} and ΔS^{rxn}) with temperature.

To better understand the temperature-dependent activity of enzymes, we used multi-temperature crystallography to reveal the structural changes of rat cytosolic PEPCK-inhibitor complexes, an extensively characterized model system. We have identified temperature-dependent changes in the active site and ligand conformations that, based on extensive prior studies, are expected to contribute to the observed increase in k_{cat} with increasing temperature at temperatures below T_{opt}. Generally, as temperature increases there is a shift from less competent to more competent active site / substrate configurations, contributing to the increase in k_{cat} (and decrease in $\Delta G^{rxn}(T)$) observed over the same temperature range. These structural changes are observed even within temperature intervals where the corresponding E-P plots appear linear. At the highest temperature probed, weak evidence for increased disorder of the active site lid suggests a shift in this equilibrium back toward chemically incompetent enzyme states, that in turn may be the origin of the negative Arrhenius curvature and loss of activity at higher temperatures.

Motivated by these and previous structural observations, it is clear than the assumption of temperature-independent parameters (E_a, A or $\Delta H^{rxn}, \Delta S^{rxn}$) when interpreting Arrhenius or Eyring-Polanyi fits will in general be invalid, even when fitting temperature intervals over which plotted data appears linear. As will be shown elsewhere, small temperature variations of E_a and ΔG^{rxn} will have large and correlated effects on the slope and intercept – on E_a^{app} / $\Delta H^{rxn,app}$ and A^{app} / $\Delta S^{rxn,app}$, muddling their mechanistic significance. Effects of these temperature variations may be so large as to render comparisons of fit parameters $\Delta H^{rxn,app}$ and $\Delta S^{rxn,app}$ obtained from related enzymes, including engineered enzymes and enzymes adapted to different thermal environments, largely meaningless unless observed differences are supported by complementary measurements. Our results point to a key role for atomic resolution multi-temperature structural

studies in illuminating fundamental aspects of structure-function relationships, protein design, and thermal adaptation.

Scheme 1: Rat cytosolic PEPCK reaction mechanism and inhibitor complexes.

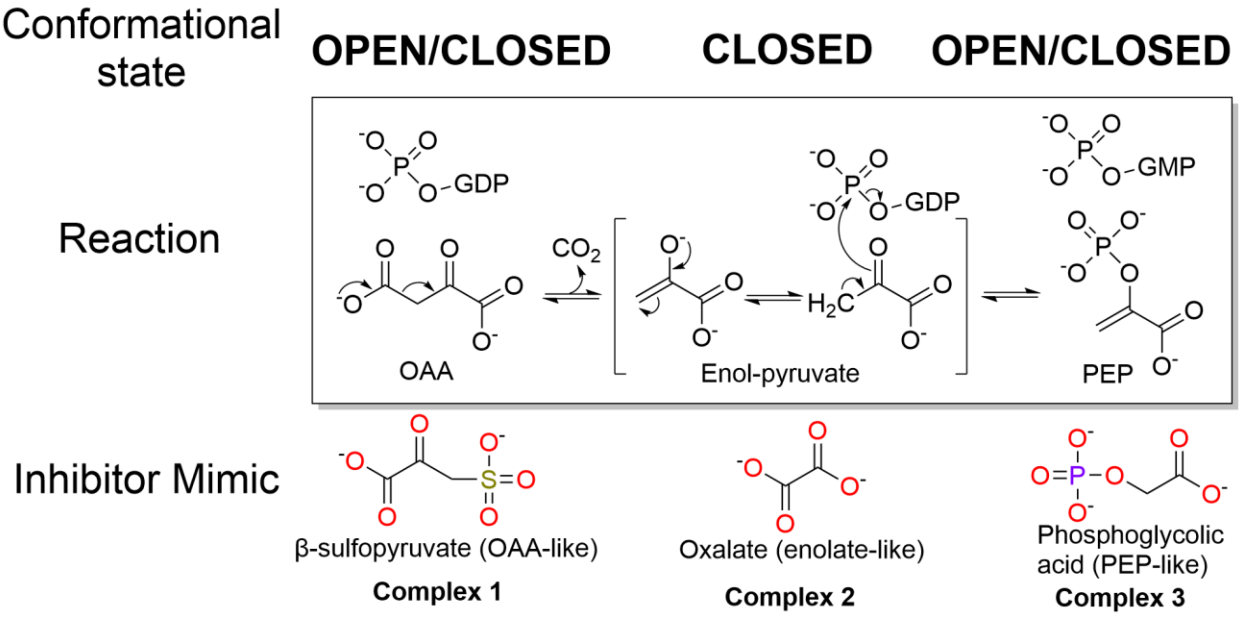

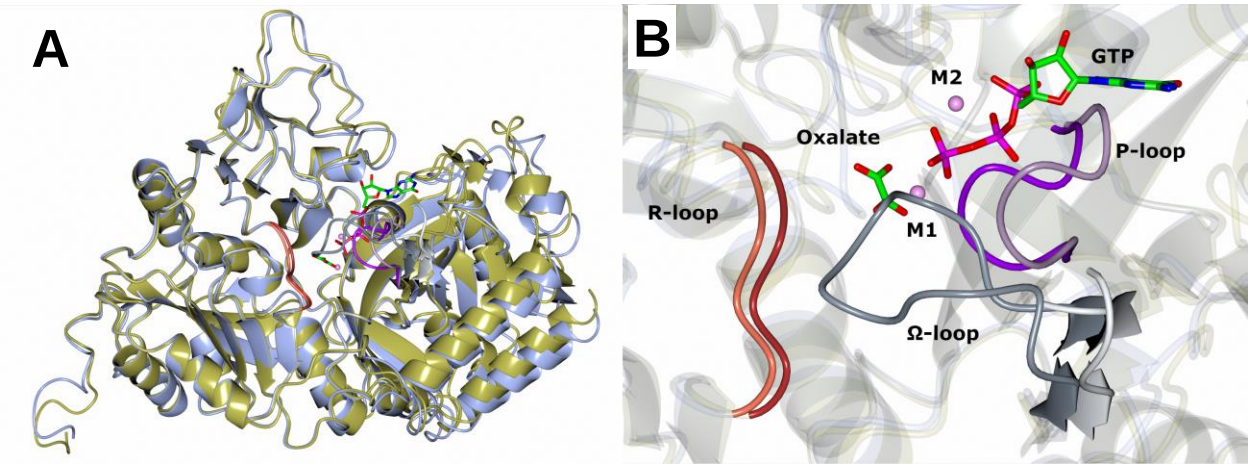

Fig. 1. Open and closed conformations of rcPEPCK along the reaction coordinate. Superposition of the open and closed structures (N-terminal domain residues 3-250) of rcPEPCK, indicating conformational changes of A) the global structure and B) the active site. Holo rcPEPCK (open) is shown in steel blue (PDB 2QEW), and its Ω-loop in light grey, R-loop in coral, and P-loop in lilac. Oxalate- (enol-pyruvate intermediate mimic) GTP bound rcPEPCK (closed) is shown in gold (PDB 3DT2) and its Ω-loop in grey, R-loop in firebrick red, and P-loop in purple. Oxalate and GTP are shown bound to the active site and atoms are colored by type (red – oxygen, blue – nitrogen, green – carbon, purple – phosphorous, pink – manganese).

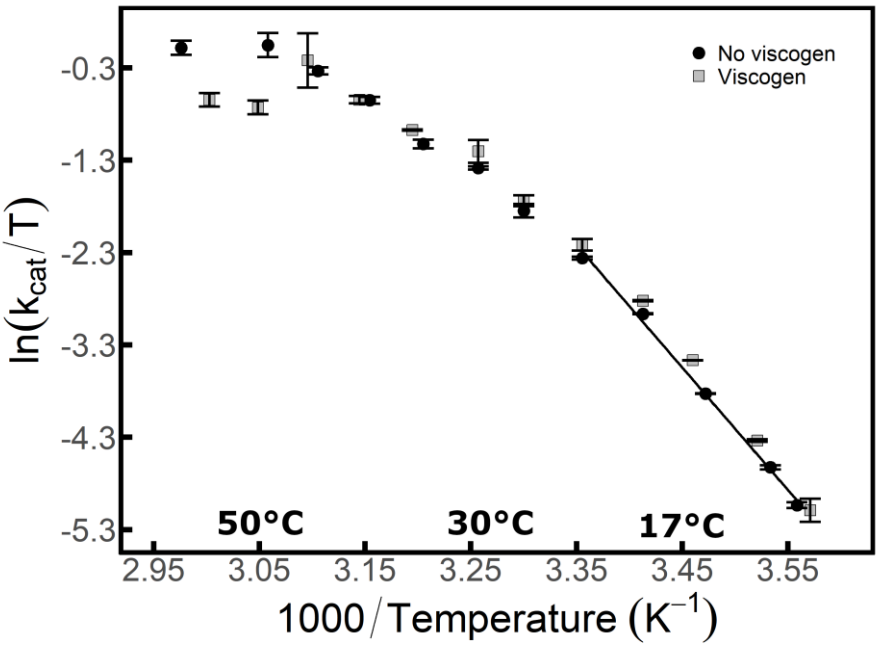

Fig. 2. Eyring-Polanyi plot for rcPEPCK mediated carboxylation of PEP. Reaction rate vs. temperature at saturating concentrations of substrate without (black circle) and with viscogen (grey squares). Linear fit corresponds to 8-25°C temperature range. Error bars (standard error) may be hidden within the data point.

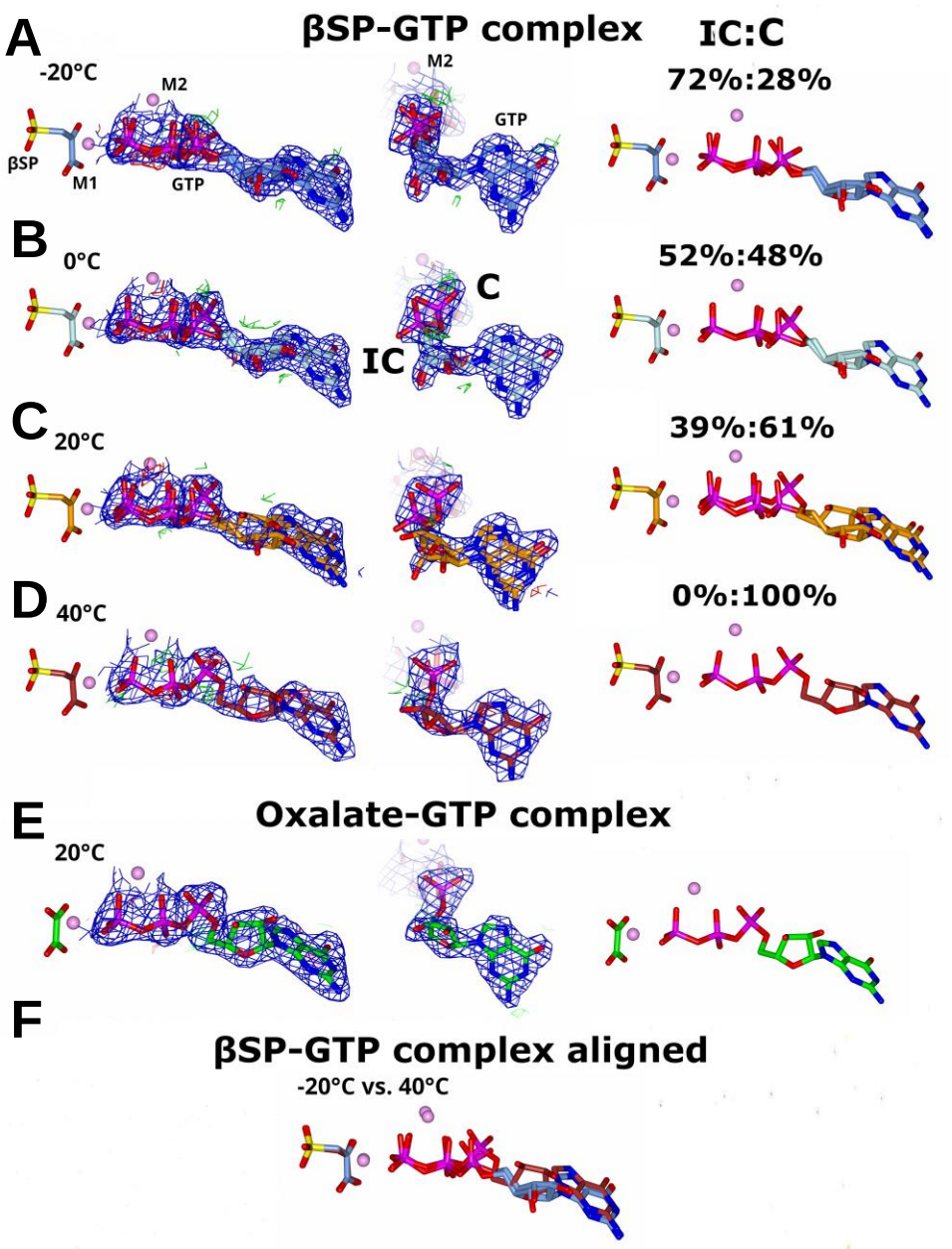

Fig. 3. Conformational change toward intermediate state with increasing temperature in the βSP-GTP (forward reaction GS) complex. Structures determined at A) -20°C (carbon – ice blue), B) 0°C (light blue), C) 20°C (orange), and D) 40°C (firebrick red) show a shift in GTP conformation as temperature is increased from the fixed, incompetent position to the rotated, competent one (IC and C respectively). The middle panel shows the same structure rotated 90° (looking in-line with nucleotide) to show conformational changes of the α-phosphate. The right panel shows the modeling without electron density with the refined occupancy values for each conformer. Specifically, the α-phosphate and ribose rotate away from the in-line plane of the triphosphate tail. At 40°C, the conformation of the nucleotide is almost identical to E) the 20°C intermediate complex (green – oxalate-GTP). F) Alignment of -20°C and 40°C structures showing the extent of the conformational change. All other atoms are colored by atom-type. Both $2F_o–F_c$ (blue – 1σ) and $F_o–F_c$ (green and red – 3σ) electron density maps are shown.

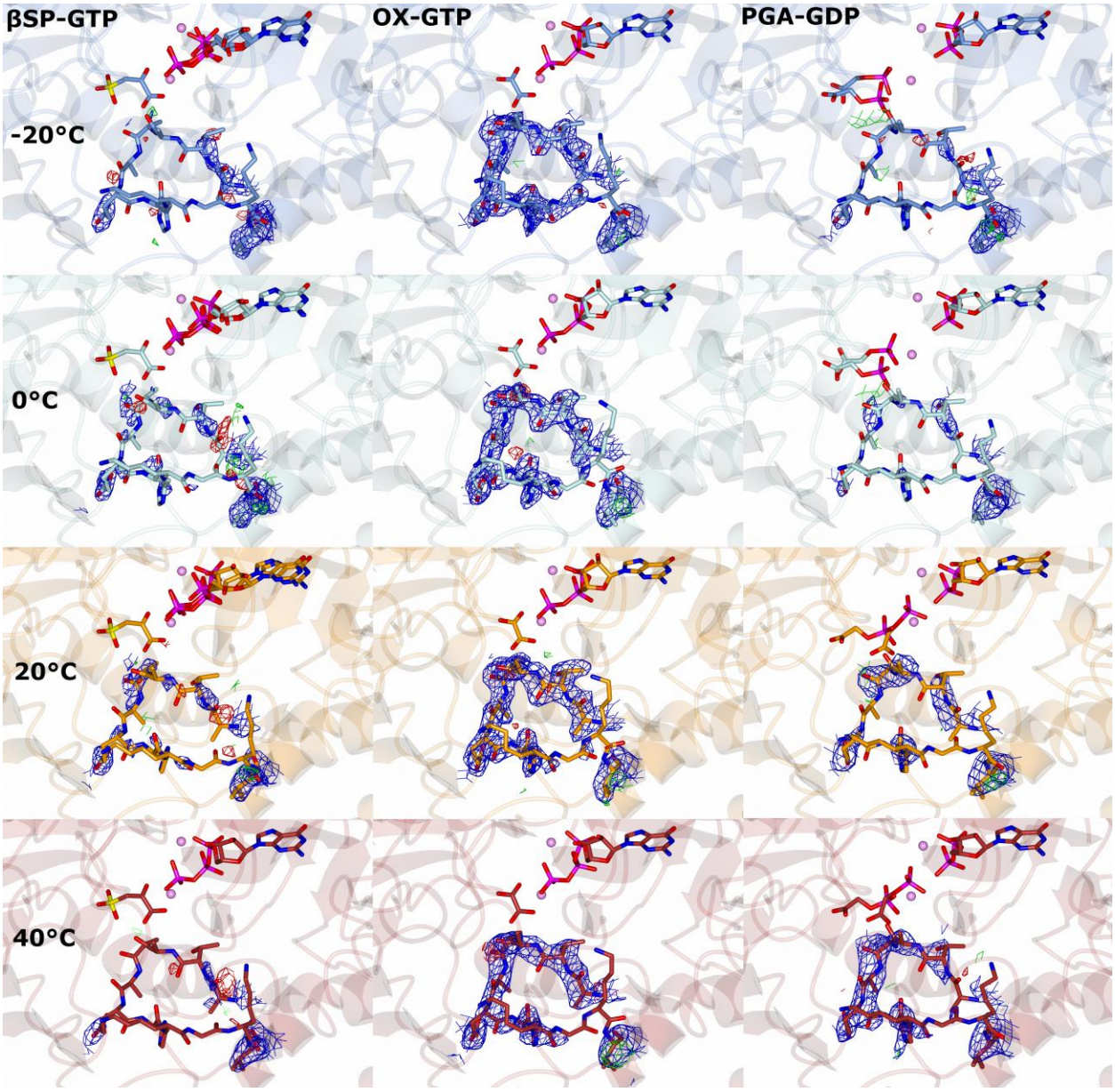

Fig. 4. Changes in Ω-loop closed conformation occupancy. In each complex, the Ω-loop is modelled in the closed conformation with an occupancy of 1.0. The $2F_o–F_c$ (blue) and $F_o–F_c$ (red/green) maps resulting from refinement are contoured to 1σ and 3σ, respectively. In the βSP-GTP complex, the closed-conformation occupancy of the Ω-loop increases from -20°C to 20°C, and then shows weak evidence of opening/disordering by 40°C (**Fig. S4**). In the oxalate-GTP complex, the Ω-loop is mostly closed at all temperatures. In the PGA-GDP complex, the closed conformation occupancy of the Ω-loop increases with increasing temperature.

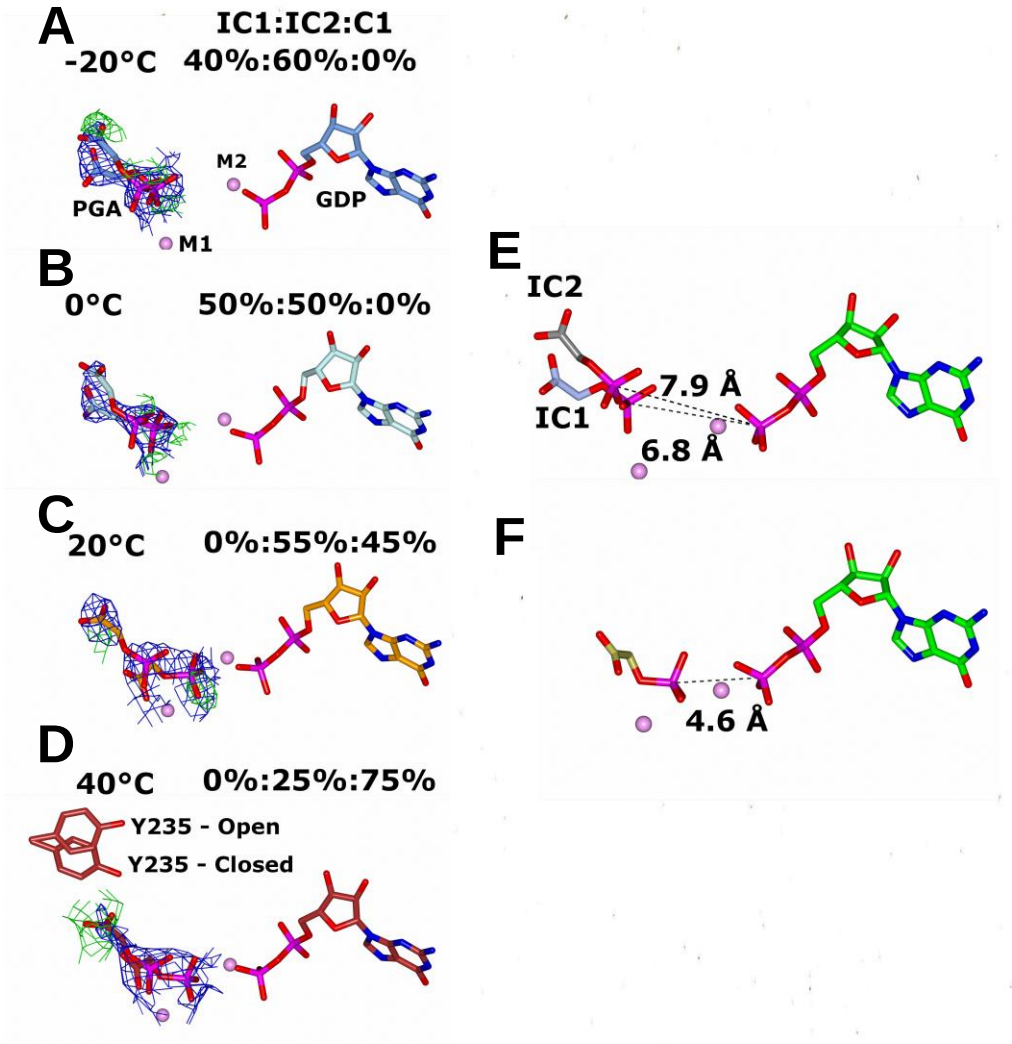

Fig. 5. Electron density maps for PGA indicate substrate conformational change with temperature. Model and electron density difference maps at A) -20°C, B) 0°C, C) 20°C, D) 40°C. PGA was observed in three distinct conformations: E) two incompetent outer shell states (IC1 and IC2; PGA-GDP P-P interatomic distances of 7.94 and 6.84 Å) and F) one competent state coordinating directly to the M1 metal (C1; P-P interatomic distance 4.84 Å) (**Fig. S1)**. As temperature increased, the relative population of the competent conformation increased. Each occupancy was manually refined to minimize the difference density present and the resultant occupancies are labeled (IC1:IC2:C1) for each panel. Y235 is shown in D) indicating the coupled conformational change of the active site with PGA/PEP location. The final $2F_o$-F_c maps (blue) are contoured to 1σ, and F_o-F_c (red/green) maps are contoured to 3σ. Positive difference density in D) surrounding IC2 was unchanging as its occupancy is increased.

References:

1. Hobbs JK, Jiao W, Easter AD, Parker EJ, Schipper LA, Arcus VL. Change in Heat Capacity for Enzyme Catalysis Determines the Temperature Dependence of Enzyme Catalysed Rates. *ACS chemical biology*. 2013;(3):2388-2393. doi:10.1021/cb4005029

2. Han MH. Non-linear Arrhenius plots in temperature-dependent kinetic studies of enzyme reactions. I. Single transition processes. *Journal of Theoretical Biology*. 1972;35:543-568. doi:10.1016/0022-5193(72)90150-6

3. Struvay C, Feller G. Optimization to low temperature activity in psychrophilic enzymes. *International Journal of Molecular Sciences*. 2012;13(9):11643-11665. doi:10.3390/ijms130911643

4. Lee CK, Daniel RM, Shepherd C, et al. Eurythermalism and the temperature dependence of enzyme activity. *The FASEB Journal*. 2007;21(8):1934-1941. doi:10.1096/fj.06-7265com

5. Truhlar DG, Kohen A. Convex Arrhenius plots and their interpretation. *Proceedings of the National Academy of Sciences of the United States of America*. 2001;98(3):848-851. doi:10.1073/pnas.98.3.848

6. Roy S, Schopf P, Warshel A. Origin of the Non-Arrhenius Behavior of the Rates of Enzymatic Reactions. *Journal of Physical Chemistry B*. 2017;121(27):6520-6526. doi:10.1021/acs.jpcb.7b03698

7. Daniel RM, Danson MJ, Eisenthal R. The temperature optima of enzymes: A new perspective on an old phenomenon. *Trends in Biochemical Sciences*. 2001;26(4):223-225. doi:10.1016/S0968-0004(01)01803-5

8. Arcus VL, Mulholland AJ. Temperature, Dynamics, and Enzyme-Catalyzed Reaction Rates. *Annu Rev Biophys*. 2020;49:163-180. doi:10.1146/annurev-biophys-121219

9. Arcus VL, Prentice EJ, Hobbs JK, et al. On the Temperature Dependence of Enzyme-Catalyzed Rates. *Biochemistry*. 2016;55(12):1681-1688. doi:10.1021/acs.biochem.5b01094

10. Van Der Kamp MW, Prentice EJ, Kraakman KL, Connolly M, Mulholland AJ, Arcus VL. Dynamical origins of heat capacity changes in enzyme-catalysed reactions. *Nature Communications*. 2018;9(1):1-7. doi:10.1038/s41467-018-03597-y

11. Walker EJ, Hamill CJ, Crean R, et al. Cooperative Conformational Transitions Underpin the Activation Heat Capacity in the Temperature Dependence of Enzyme Catalysis. *ACS Catal*. 2024;14(7):4379-4394. doi:10.1021/acscatal.3c05584

12. Åqvist J, Sočan J, Purg M. Hidden Conformational States and Strange Temperature Optima in Enzyme Catalysis. *Biochemistry*. 2020;59(40):3844-3855. doi:10.1021/acs.biochem.0c00705

13. Åqvist J, Van Der Ent F. Calculation of Heat Capacity Changes in Enzyme Catalysis and Ligand Binding. *Journal of Chemical Theory and Computation*. 2022;18(10):6345-6353. doi:10.1021/acs.jctc.2c00646

14. Daniel RM, Danson MJ. Temperature and the catalytic activity of enzymes: A fresh understanding. *FEBS Letters*. 2013;587(17):2738-2743. doi:10.1016/j.febslet.2013.06.027

15. Clarke A. The thermal limits to life on Earth. *International Journal of Astrobiology*. 2014;13(02):141-154. doi:10.1017/S1473550413000438

16. Warkentin M, Thorne RE. Glass transition in thaumatin crystals revealed through temperature-dependent radiation-sensitivity measurements. *Acta Crystallographica Section D: Biological Crystallography*. 2010;66(10):1092-1100. doi:10.1107/S0907444910035523

17. Warkentin M, Thorne RE. Slow cooling of protein crystals. *Journal of Applied Crystallography*. 2009;42(5):944-952. doi:10.1107/S0021889809023553

18. Doukov T, Herschlag D, Yabukarski F. Instrumentation and experimental procedures for robust collection of X-ray diffraction data from protein crystals across physiological temperatures. *Journal of Applied Crystallography*. 2020;53:1493-1501. doi:10.1107/S1600576720013503

19. Keedy DA, Hill ZB, Biel JT, et al. An expanded allosteric network in PTP1B by multitemperature crystallography, fragment screening, and covalent tethering. *eLife*. 2018;7:1-36. doi:10.7554/eLife.36307.001

20. Keedy DA, Kenner LR, Warkentin M, et al. Mapping the conformational landscape of a dynamic enzyme by multitemperature and XFEL crystallography. *eLife*. 2015;4:1-26. doi:10.7554/eLife.07574

21. Fraser JS, Van Den Bedem H, Samelson AJ, et al. Accessing protein conformational ensembles using room-temperature X-ray crystallography. *Proceedings of the National Academy of Sciences of the United States of America*. 2011;108(39):16247-16252. doi:10.1073/pnas.1111325108

22. Tilton RF, Dewan JC, Petsko GA. Effects of Temperature on Protein Structure and Dynamics: X-ray Crystallographic Studies of the Protein Ribonuclease-A at Nine Different Temperatures from 98 to 320 K. *Biochemistry*. 1992;31(9):2469-2481. doi:10.1021/bi00124a006

23. Fraser JS, Clarkson MW, Degnan SC, Erion R, Kern D, Alber T. Hidden alternative structures of proline isomerase essential for catalysis. *Nature*. 2009;462(7273):669-673. doi:10.1038/nature08615

24. Stachowski TR, Vanarotti M, Seetharaman J, Lopez K, Fischer M. Water Networks Repopulate Protein–Ligand Interfaces with Temperature. *Angew Chem Int Ed*. 2022;61(31). doi:10.1002/anie.202112919

25. Bradford SYC, El Khoury L, Ge Y, Osato M, Mobley DL, Fischer M. Temperature artifacts in protein structures bias ligand-binding predictions. *Chem Sci*. 2021;12(34):11275-11293. doi:10.1039/D1SC02751D

26. Dong M, Lauro ML, Koblish TJ, Bahnson BJ. Conformational sampling and kinetics changes across a non-Arrhenius break point in the enzyme thermolysin. *Structural Dynamics*. 2020;7(1). doi:10.1063/1.5130582

27. Guerrero L, Ebrahim A, Riley BT, et al. Pushed to extremes: distinct effects of high temperature versus pressure on the structure of STEP. *Commun Biol*. 2024;7(1):59. doi:10.1038/s42003-023-05609-0

28. Sullivan SM, Holyoak T. Enzymes with lid-gated active sites must operate by an induced fit mechanism instead of conformational selection. *Proceedings of the National Academy of Sciences*. 2008;105(37):13829-13834. doi:10.1073/pnas.0805364105

29. Sullivan SM, Holyoak T. Structures of Rat Cytosolic PEPCK: Insight into the Mechanism of Phosphorylation and Decarboxylation of Oxaloacetic Acid. *Biochemistry*. 2007;46(35):10078-10088. doi:10.1021/bi701038x

30. Carlson GM, Holyoak T. Structural insights into the mechanism of phosphoenolpyruvate carboxykinase catalysis. *J Biol Chem*. 2009;284(40):27037-27041. doi:10.1074/jbc.R109/040568

31. Johnson TA, Holyoak T. The Ω-loop Lid Domain of Phosphoenolpyruvate Carboxykinase is Essential for Catalytic Function. *Biochemistry*. 2012;51(47):9547-9559. doi:10.1021/bi301278t

32. Holyoak T, Sullivan SM, Nowak T. Structural Insight into the Mechanism of PEPCK Catalysis. *Biochemistry*. 2006;45(27):8254-8263. doi:10.1021/bi060269g

33. Johnson TA, Mcleod MJ, Holyoak T. Utilization of Substrate Intrinsic Binding Energy for Conformational Change and Catalytic Function in Phosphoenolpyruvate Carboxykinase. *Biochemistry*. 2016;55(3):575-587. doi:10.1021/acs.biochem.5b01215

34. Clinger JA, Moreau DW, McLeod MJ, Holyoak T, Thorne RE. Millisecond mix-and-quench crystallography (MMQX) enables time-resolved studies of PEPCK with remote data collection. *IUCrJ*. 2021;8(5):784-792. doi:10.1107/s2052252521007053

35. McLeod MJ, Holyoak T. Phosphoenolpyruvate Carboxykinases. *Encyclopedia of Biological Chemistry III*. 2021;3:400-412. doi:10.1016/b978-0-12-819460-7.00226-7

36. Cui DS, Broom A, McLeod MJ, Meiering EM, Holyoak T. Asymmetric Anchoring is Required for Efficient Ω-Loop Opening and Closing in Cytosolic Phosphoenolpyruvate Carboxykinase. *Biochemistry*. 2017;56(15):2106-2115. doi:10.1021/acs.biochem.7b00178

37. Chen CY, Chang YC, Lin BL, Huang CH, Tsai MD. Temperature-Resolved Cryo-EM Uncovers Structural Bases of Temperature-Dependent Enzyme Functions. *Journal of the American Chemical Society*. 2019;141(51):19983-19987. doi:10.1021/jacs.9b10687

38. Singh AK, McGoldrick LL, Demirkhanyan L, Leslie M, Zakharian E, Sobolevsky AI. Structural basis of temperature sensation by the TRP channel TRPV3. *Nature Structural and Molecular Biology*. 2019;26(11):994-998. doi:10.1038/s41594-019-0318-7

39. Stiffin RM, Sullivan SM, Carlson GM, Holyoak T. Differential Inhibition of Cytosolic PEPCK by Substrate Analogues. Kinetic and Structural Characterization of Inhibitor Recognition. *Biochemistry*. 2008;47(7):2099-2109. doi:10.1021/bi7020662

40. Sudom AM, Prasad L, Goldie H, Delbaere LTJ. The Phosphoryl-transfer Mechanism of Escherichia coli Phosphoenolpyruvate Carboxykinase From the Use of AlF3. *Journal of Molecular Biology*. 2001;314:83-92. doi:10.1006/jmbi.2001.5120

41. Holyoak T, Nowak T. pH Dependence of the Reaction Catalyzed by Avian Mitochondrial Phosphoenolpyruvate Carboxykinase. *Biochemistry*. 2004;43(22):7054-7065. doi:10.1021/bi049707e

42. Johnson TA, Holyoak T. Increasing the Conformational Entropy of the Ω-Loop Lid Domain in Phosphoenolpyruvate Carboxykinase Impairs Catalysis and Decreases Catalytic Fidelity. *Biochemistry*. 2010;49(25):5176-5187. doi:10.1021/bi100399e

43. Barwell S, Duman R, Wagner A, Holyoak T. Directional regulation of cytosolic PEPCK catalysis is mediated by competitive binding of anions. *Biochemical and Biophysical Research Communications*. 2022;637:218-223. doi:10.1016/j.bbrc.2022.11.025

44. Balan MD, McLeod MJ, Lotosky WR, Ghaly M, Holyoak T. Inhibition and Allosteric Regulation of Monomeric Phosphoenolpyruvate Carboxykinase by 3-Mercaptopicolinic Acid. *Biochemistry*. 2015;54(38):5878-5887. doi:10.1021/acs.biochem.5b00822

45. Juers DH, Matthews BW. Reversible lattice repacking illustrates the temperature dependence of macromolecular interactions. *Journal of Molecular Biology*. 2001;311(4):851-862. doi:10.1006/jmbi.2001.4891

46. Skaist Mehlman T, Biel JT, Azeem SM, et al. Room-temperature crystallography reveals altered binding of small-molecule fragments to PTP1B. *eLife*. 2023;12:e84632. doi:10.7554/eLife.84632

47. Lang PT, Holton JM, Fraser JS, Alber T. Protein structural ensembles are revealed by redefining X-ray electron density noise. *Proceedings of the National Academy of Sciences of the United States of America*. 2014;111(1):237-242. doi:10.1073/pnas.1302823110

48. Nagel ZD, Dong M, Bahnson BJ, Klinman JP. Impaired protein conformational landscapes as revealed in anomalous Arrhenius prefactors. *PNAS*. 2011;108(26):10520-10525. doi:10.1073/pnas.1104989108

49. Yabukarski F, Biel JT, Pinney MM, et al. Assessment of enzyme active site positioning and tests of catalytic mechanisms through X-ray–derived conformational ensembles. *Proceedings of the National Academy of Sciences of the United States of America*. 2020;117(52):33204-33215. doi:10.1073/PNAS.2011350117

50. Frauenfelder H, Petsko GA. Structural dynamics of liganded myoglobin. *Biophysical Journal*. 1980;32:465-483. doi:10.1016/S0006-3495(80)84984-8

51. Northrop DB. On the meaning of Km and V/K in enzyme kinetics. *Journal of Chemical Education*. 1998;75(9):1153-1157. doi:10.1021/ed075p1153

52. Londesborough J. The Causes of Sharply Bent or Discontinuous Arrhenius Plots for Enzyme-Catalysed Reactions. *European Journal of Biochemistry*. 1980;105(2):211-215. doi:10.1111/j.1432-1033.1980.tb04491.x

53. Case A, Stein RL. Mechanistic origins of the substrate selectivity of serine proteases. *Biochemistry*. 2003;42(11):3335-3348. doi:10.1021/bi020668l

54. Cornish-Bowden A. Enthalpy-entropy compensation: a phantom phenomenon. *J Biosci*. 2002;27(2):121-126. doi:10.1007/BF02703768

55. Lenaz G, Sechi AM, Parenti-Castelli G, Landi L, Bertoli E. Activation Energies of Different Mitochondrial Enzymes: Breaks in Arrhenius Plots of Membrane-Bound Enzymes Occur at Different Temperatures. *Biochemical and Biophysical Research Communications*. 1972;49(2):536-542. doi:10.1016/0006-291X(72)90444-5

56. Lonhienne T, Baise E, Feller G, Bouriotis V, Gerday C. Enzyme activity determination on macromolecular substrates by isothermal titration calorimetry: application to mesophilic and psychrophilic chitinases. *Biochimica et Biophysica Acta*. 2001;1545:349-456. doi:10.1016/S0167-4838(00)00296-X

57. Allen B, Blum M, Cunningham A, Tu GC, Hofmann T. A ligand-induced, temperature-dependent conformational change in penicillopepsin. Evidence from nonlinear Arrhenius plots and from circular dichroism studies. *Journal of Biological Chemistry*. 1990;265(9):5060-5065. doi:10.1016/s0021-9258(19)34084-0

58. Silverstein TP. Falling enzyme activity as temperature rises: Negative activation energy or denaturation? *Journal of Chemical Education*. 2012;89(9):1097-1099. doi:10.1021/ed200497r

59. Lam SY, Yeung RCY, Yu TH, Sze KH, Wong KB. A rigidifying salt-bridge favors the activity of thermophilic enzyme at high temperatures at the expense of low-temperature activity. *PLoS Biology*. 2011;9(3). doi:10.1371/journal.pbio.1001027

60. Machado TFG, Gloster TM, da Silva RG. Linear Eyring Plots Conceal a Change in the Rate-Limiting Step in an Enzyme Reaction. *Biochemistry*. 2018;57(49):6757-6761. doi:10.1021/acs.biochem.8b01099

Acknowledgments: We would like to acknowledge Norman Tran for thoughtful discussions. We would also like to acknowledge CHESS staff, specifically Irina Kriksunov, Bill Miller, and David Schuller.

Funding: MJM and the experimental work at Cornell was supported by NIH award 5R01GM127528-04 and by NSF award DBI-2210041.

T.H acknowledges support from the Natural Science and Engineering Research Council (NSERC) of Canada.

CHEXS is supported by the NSF award DMR-1829070, and the MacCHESS resource is supported by NIGMS award 1-P30-GM124166-01A1 and NYSTAR.

Author contributions:

Conceptualization: MJM, TH, RET

Methodology: MJM, SB, RET

Investigation: MJM, SB, RET

Expression/Purification: MJM, SB

Kinetics: MJM

Crystallography: MJM

Analysis: MJM, RET

Visualization: MJM

Funding acquisition: TH, RET

Project administration: TH, RET

Supervision: TH, RET

Writing – original draft: MJM, RET

Writing – review & editing: MJM, RET, TH

Competing interests: RET is majority owner and CTO of MiTeGen, which manufactures and sells some of the tools used in this research.

Data and materials availability: Structural datasets are deposited in the PDB (accession numbers found in **Table S3-5**) and all other data can be made available.